CrystEngComm

PAPER

View Article Online
View Journal | View Issue

Cite this: *CrystEngComm*, 2014, **16**, 1296

Controllable synthesis of $NH_4Eu_3F_{10}$ nanospheres and application in bioimaging†

Zhiyang Zhang,[a] Xiaoyan Ma,[a] Zhiming Chen,[ab] Kuaibing Wang,[ac] Yidan Wang,[a] Zhirong Geng*[a] and Zhilin Wang*[a]

Received 28th October 2013,
Accepted 30th October 2013

DOI: 10.1039/c3ce42193g

www.rsc.org/crystengcomm

Cubic phase $NH_4Eu_3F_{10}$ nanospheres with controllable sizes were synthesized *via* a modified hydrothermal route by varying the dosage of ammonium hydroxide solution. Dependence of structure and morphology on the dosage of ammonia water and reaction time were investigated by X-ray powder diffraction (XRD) and transmission electron microscopy (TEM). Being unstable, $NH_4Eu_3F_{10}$ decomposed into EuF_3 and NH_4F during the long-time hydrothermal treatment. EDTA, as the chelation agent of Eu^{3+} and the capping ligand on the surface of as-obtained nanospheres, showed different chelating abilities depending on the dosage of ammonium hydroxide solution. Increasing the amount of ammonia not only decreased the effective concentration of Eu^{3+}, but also decelerated the growth of $NH_4Eu_3F_{10}$ nanospheres and stabilized them by reducing the surface energy. Given the satisfactory hydrophilicity, biocompatibility, and luminescence, the as-obtained nanospheres were applied as promising agents for cell imaging by presenting high contrast.

Introduction

Recently, photoluminescence nano- and micro-materials of rare-earth fluorides have attracted considerable interest due to their unique luminescence properties originating from f–f electronic transitions within 4f electrons of rare-earth ions. As a familiar host matrix, rare-earth fluorides provide low nonradiative relaxation and high quantum efficiency by having low vibrational energies.[1,2] Compared with conventional luminescent probes such as organic fluorescent dyes and quantum dots, rare-earth fluorides exhibit higher photostability and chemical stability.[3] In addition, rare-earth fluorides are biocompatible, thus making them applicable to bioimaging, biochemical probing, and drug delivery, *etc.*[4–9]

Up to now, an important family of rare-earth fluorides, MLn_3F_{10} (M = alkali metal and Ln = rare earth), such as KYb_3F_{10}, $RbGd_3F_{10}$ and $CsYb_3F_{10}$, *etc.*,[10–13] have been studied. Generally, the formation of MLn_3F_{10} depends strongly on the size of cation.[14] For instance, Vedrine *et al.*[15] proposed that cubic $RbLn_3F_{10}$ was obtained only in the narrow range of $1.41 < R < 1.49$ ($R = r_{M^+}/r_{Ln^{3+}}$). You *et al.*[16] reported that LnF_3 usually formed for larger rare earth cations (La^{3+}, Pr^{3+} and Nd^{3+}), $RbLn_2F_7$ was obtained in the case of smaller cations (Yb^{3+} and Lu^{3+}), and $RbLn_3F_{10}$ formed only in the range of $1.42 < R < 1.55$ which was close to the result reported by Vedrine.[15] The ionic radius (Pauling) of NH_4^+ is 1.48 Å which is comparable with those of K^+ (1.33 Å) and Rb^+ (1.48 Å).[17] Thus, $NH_4Ln_3F_{10}$ are bound to form following the same rules as the similarly structured fluorides. Liang *et al.*[18] synthesized a series of $NH_4Ln_3F_{10}$ (Ln = Gd, Tb, Dy). LnF_3 (Ln = La, Ce, Nd, Pr, Sm, Eu) was obtained for the larger cations, and $NH_4Ln_2F_7$ (Ln = Y, Ho, Er, Tm, Yb, Lu) formed when the cations were smaller. The results are similar to those of RbF–LnF_3 in a previous report.[16] Kang *et al.*[17] synthesized $NH_4Ln_3F_{10}$ (Ln = Dy, Ho, Y, Er, Tm), and further pointed out that larger rare earth cations tended to form LnF_3 (Ln = La, Nd, Eu, Gd) instead of $NH_4Ln_3F_{10}$ by being highly unstable. In addition, these as-prepared $NH_4Ln_3F_{10}$ were prone to decomposition at high temperature. The ionic radius of Eu^{3+} is larger than that of Gd^{3+} which is the largest rare earth cation forming $NH_4Ln_3F_{10}$ to date, thus rendering $NH_4Eu_3F_{10}$ difficult to prepare as larger rare earth cations are more unstable. To the best of our knowledge, pure $NH_4Eu_3F_{10}$ has never been successfully synthesized, and most $NH_4Ln_3F_{10}$ available hitherto are not in uniform nano-sizes. Therefore,

[a] *State Key Laboratory of Coordination Chemistry, School of Chemistry and Chemical Engineering, Nanjing University, Nanjing 210093, PR China. E-mail: wangzl@nju.edu.cn, gengzr@nju.edu.cn; Fax: +86 25 83317761; Tel: +86 25 83686082*
[b] *Department of Biochemical Engineering, Anhui Polytechnic University, Wuhu 241000, PR China*
[c] *School of Science, Nanjing Agricultural University, Nanjing 210095, PR China*

† Electronic supplementary information (ESI) available: XRD patterns for products prepared in 5.5 mL of ammonium hydroxide solution without EDTA or oleic acid, and for products prepared in 9.5 mL of and 10.0 mL of ammonium hydroxide solutions, luminescence spectrum for as-obtained $NH_4Eu_3F_{10}$ nanospheres, MTT assay for $NH_4Eu_3F_{10}$ nanospheres, CLFM images of HeLa cells incubated with $NH_4Eu_3F_{10}$ nanospheres for various times. See DOI: 10.1039/c3ce42193g

fabricating $NH_4Eu_3F_{10}$ nanoparticles with controlled size is significant. Herein we synthesized cubic phase $NH_4Eu_3F_{10}$ nanospheres through a modified hydrothermal route we have reported previously.[19]

In this paper, for the first time, cubic phase $NH_4Eu_3F_{10}$ nanospheres with controlled sizes were synthesized based on a modified hydrothermal method by varying the amount of ammonia. Dependence of the products on the concentration of ammonium hydroxide solution was studied systematically. A rational theory was proposed to explain the variation of products induced by varying the amount of ammonia. Ammonia affected the deprotonation and chelation of EDTA, which influenced the growth rate of nanoparticles by affecting the effective concentration of Eu^{3+}. Besides, the pH value, which determined the capping ligands on the surface of as-prepared nanospheres, was also varied by changing the amount of ammonia. Sizes of $NH_4Eu_3F_{10}$ nanospheres can also be adjusted by varying the dosage of ammonia after reaction for 1 h. Being luminescent, biocompatible and hydrophilic, the small-sized as-prepared nanospheres are particularly suitable for cell imaging *in vitro*.

Experimental

Preparation of $NH_4Eu_3F_{10}$ nanospheres

$NH_4Eu_3F_{10}$ nanospheres were prepared by the following procedures. Eu_2O_3 (176 mg) was dissolved in 5 mL of nitric acid solution (1 M) and with addition of 2 mL of ammonium hydroxide solution (1 M), 5 mL of oleic acid, and 5 mL of absolute ethanol to obtain solution A. Then the solution was dispersed by sonolysis for 5 min. Solution B was obtained by dissolving 500 mg EDTA and 200 mg NH_4F in 9.1 mL of ammonium hydroxide solution (1 M). Solutions A and B were mixed and added to 5 mL of absolute ethanol. After ultrasonication for 5 min, the mixture was transferred into a 50 mL Teflon-lined stainless steel autoclave and heated at 110 °C for 8 h. After the autoclave was cooled to room temperature in a drying oven, white powder was collected by centrifugation, washed with distilled water and absolute ethanol several times, and finally dried at 100 °C in air for 3 h.

Cytotoxicity assay

The cytotoxicity of $NH_4Eu_3F_{10}$ was measured by the 3-(4,5-dimethylthiazol-2-yl)-2,5-diphenyltetrazolium bromide (MTT) assay against HeLa cells. HeLa cells were seeded in 96-well plates at 2×10^4 cells per well in culture medium and incubated for 12 h, to which were then added different quantities of the as-obtained $NH_4Eu_3F_{10}$ nanospheres. The cells were subsequently incubated for 24 or 48 h. Thereafter, 20 μL of MTT (final concentration: 5 mg mL^{-1}) was added to these wells, and then the mixture was incubated for another 4 h. After replacing the culture medium with dimethyl sulfoxide (DMSO), the absorbance of MTT formazan was monitored at 570 nm using an automatic enzyme-linked immunosorbent assay plate reader. The cytotoxicity was manifested as the percentage of cell viability.

Confocal laser fluorescence microscope (CLFM) imaging *in vitro*

In a typical procedure, 2×10^4 human cervical cancer cells (HeLa cells) were plated in a 35 mm Petri dish overnight until attachment. Then the cells were washed with phosphate-buffered saline (PBS) twice, and incubated in a culture medium containing 100 μg mL^{-1} $NH_4Eu_3F_{10}$ nanospheres for 0.5–48 h at 37 °C under 5% CO_2. After being washed with PBS several times to remove excess materials, the cells were observed under a confocal laser fluorescence microscope at the excitation wavelength of 405 nm.

Characterizations

X-ray powder diffraction (XRD) of the products were measured by a Bruker D8 Advance instrument with Cu Kα radiation (λ = 0.15406 nm) in the 2θ range from 15 to 80°. Morphologies of the as-prepared samples were observed with an Hitachi S-4800 field-emission scanning electron microscope (FE-SEM). Transmission electron microscopy (TEM) was measured on a JEM-1011 instrument microscope at an acceleration voltage of 100 kV. Down-conversion luminescent spectra were captured on a Hitachi F-4600 luminescence spectrometer. Infrared spectroscopic analysis was carried out by using a Bruker IR vector22 infrared spectrometer. Fluorescence microscope images were acquired on a Zeiss LSM 710 confocal laser fluorescence microscope. X-ray photoelectron spectroscopy (XPS spectra) was obtained on Thermo Scientific K-Alpha equipment, and the binding energy was referred to the C 1s photoelectron peak.

Results and discussion

$NH_4Eu_3F_{10}$ nanospheres were prepared by a modified hydrothermal treatment in the presence of 9.1 mL of 1 M ammonium hydroxide solution in solution B (also the amounts of ammonium hydroxide solution below). The product was characterized by XRD, TEM and SEM (Fig. 1). XRD patterns of the as-obtained product shown (Fig. 1a) can be assigned to cubic phase $NH_4Eu_3F_{10}$.[17,18] TEM (Fig. 1b) and SEM (Fig. 1c) images reveal that the $NH_4Eu_3F_{10}$ nanospheres were monodisperse with an average diameter of 114.5 ± 18.5 nm. Rietveld refinement on the finely scanned XRD patterns of the as-prepared sample confirmed that the $NH_4Eu_3F_{10}$ nanospheres crystallized in the cubic $NH_4Y_3F_{10}$ structure type (R_p = 0.059, R_{wp} = 0.11). The lattice constants of cubic $NH_4Eu_3F_{10}$ are $a = b = c$ = 11.63696 Å. As $NH_4Eu_3F_{10}$ is isostructural with the cubic $NH_4Y_3F_{10}$, they should share the same space group of $Fm\bar{3}m$.[20,21]

The dependence of crystal structure and morphology of the as-prepared europium fluorides on the amount of ammonium were studied simultaneously. Fig. 2a shows the XRD patterns of the products derived from the mother liquor containing 6.0 mL of 1 M ammonium hydroxide solution. The diffraction peaks can be indexed to hexagonal phase EuF_3 (JCPDS 32-0373). With 6.5 mL of ammonia, cubic phase

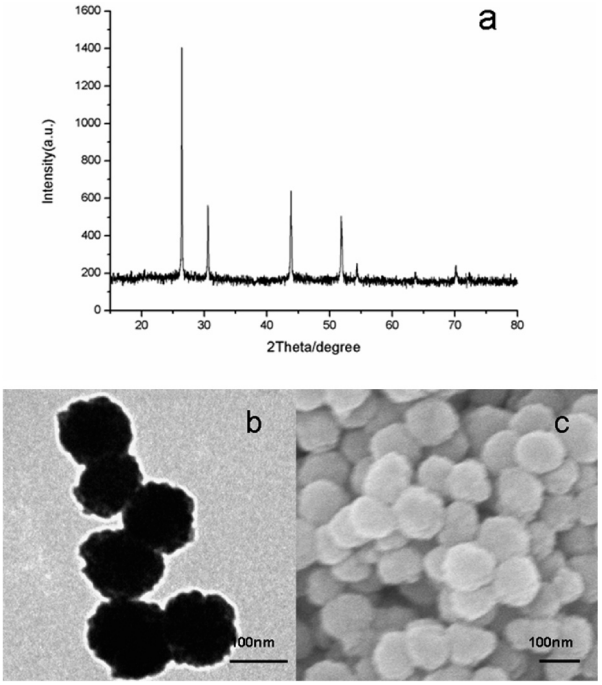

Fig. 1 (a) XRD patterns of as-prepared $NH_4Eu_3F_{10}$ nanospheres, (b) and (c) TEM and SEM images of products, respectively.

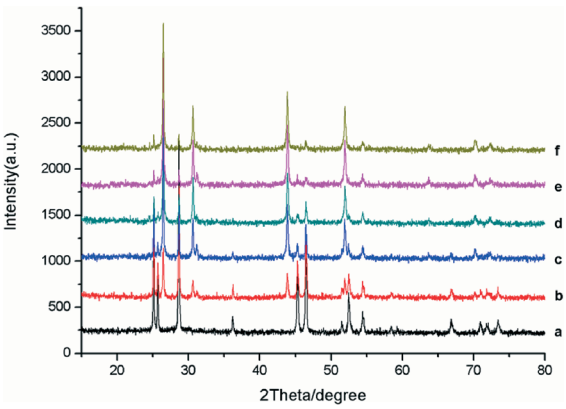

Fig. 2 XRD patterns of products prepared at 110 °C for 8 h with different amounts of ammonium hydroxide solution (a) 6.0 mL, (b) 6.5 mL, (c) 7.0 mL, (d) 7.5 mL, (e) 8.0 mL and (f) 8.5 mL.

$NH_4Eu_3F_{10}$ appeared (Fig. 2b), which increased as the ammonia amount was elevated (Fig. 2c–f). Upon addition of 9.1 mL of ammonium hydroxide solution, pure cubic phase $NH_4Eu_3F_{10}$ was obtained as presented in Fig. 1a.

Fig. 3 and Fig. 4 show the TEM and SEM images of corresponding products. Only hexagonal prisms assigned to hexagonal phase EuF_3 were observed (Fig. 3a and Fig. 4a).[19] Hexagonal prisms gradually reduced with increasing amounts of ammonium hydroxide solution (Fig. 3b–f and Fig. 4b–f), and nanospheres assigned to the cubic phase $NH_4Eu_3F_{10}$ increased until few hexagonal prisms remained.

Curves a and b show the XPS spectra of as-obtained EuF_3 and $NH_4Eu_3F_{10}$ respectively (Fig. 5). No nitrogen was detected in EuF_3 samples. Compared with that of EuF_3, the nitrogen

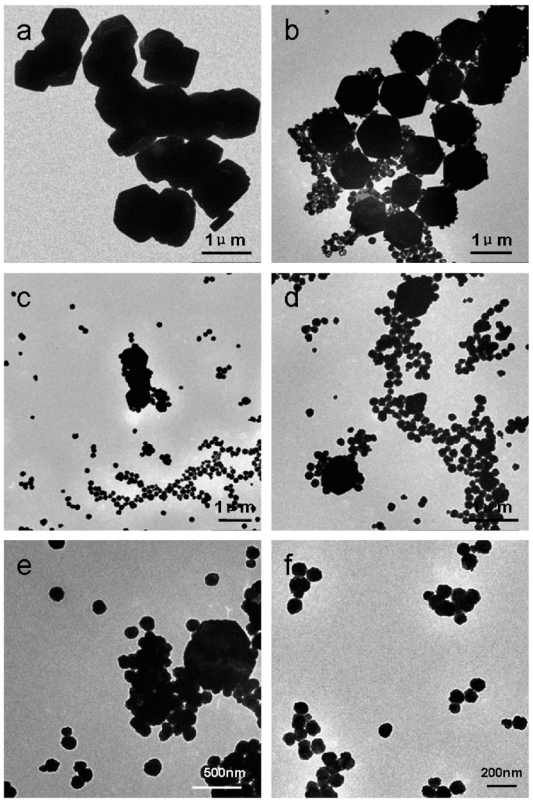

Fig. 3 TEM images of products at 110 °C for 8 h with different amounts of ammonium hydroxide solution: (a) 6.0 mL, (b) 6.5 mL, (c) 7.0 mL, (d) 7.5 mL, (e) 8.0 mL and (f) 8.5 mL.

content of $NH_4Eu_3F_{10}$ was higher, and the peaks of Eu $3d_{5/2}$ spectrum slightly negatively shifted, which can be ascribed to the variation of electron cloud density on Eu^{3+} due to the difference between the bonds of Eu–F in EuF_3 and $NH_4Eu_3F_{10}$.[22–25] The results resemble those of EuF_3:Tb^{3+} and EuF_3:Tb^{3+}/NH_4^+ hollow sub-microstructures we previously reported.[26] The ratio of N, Eu and F detected by XPS is 3.7 : 11.0 : 31.4, which is approximate to the stoichiometric ratio 1 : 3 : 10 of $NH_4Eu_3F_{10}$, and further confirms the preparation of $NH_4Eu_3F_{10}$.

Time gradient experiments indicate that the initial product was cubic phase $NH_4Eu_3F_{10}$, and hexagonal phase EuF_3 which appeared more stable when the reaction time was prolonged. With 5.5 mL of ammonia, the as-prepared sample was $NH_4Eu_3F_{10}$ after being treated hydrothermally for 1 h (Fig. 6a). EuF_3 appeared after 2 h of reaction (Fig. 6b), which increased with elapsed reaction time (Fig. 6c and d). Pure hexagonal phase EuF_3 was obtained when the reaction was prolonged to 8 h (Fig. 6e). Raising the dosage of ammonium hydroxide solution to 9.1 mL led to similar results. $NH_4Eu_3F_{10}$ predominated in the first 12 h, (Fig. 7a–e), and EuF_3 appeared after 13 h treatment (Fig. 7f). More EuF_3 was detected as the reaction was prolonged (Fig. 7g and h). As a result, in our synthetic system, $NH_4Eu_3F_{10}$ which formed at first was prone to decomposition and transformation into hexagonal phase EuF_3 during the long hydrothermal treatment time. The amount of ammonium hydroxide solution

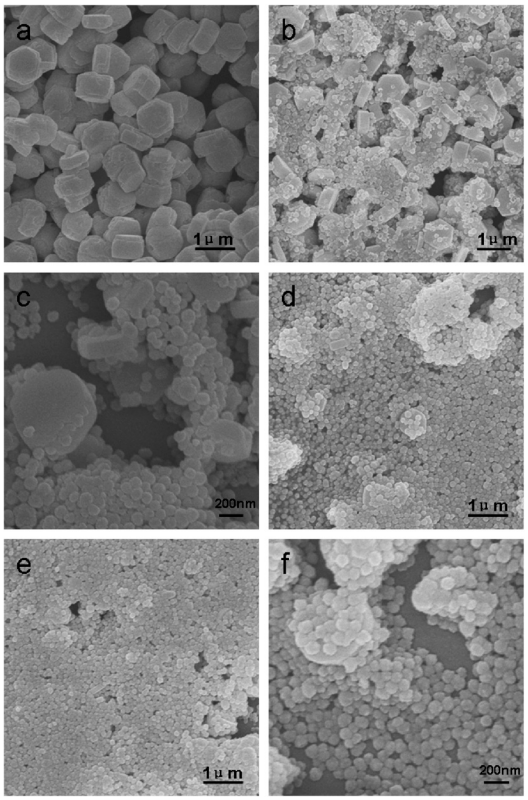

Fig. 4 SEM images of products at 110 °C for 8 h with different amounts of ammonium hydroxide solution: (a) 6.0 mL, (b) 6.5 mL, (c) 7.0 mL, (d) 7.5 mL, (e) 8.0 mL and (f) 8.5 mL.

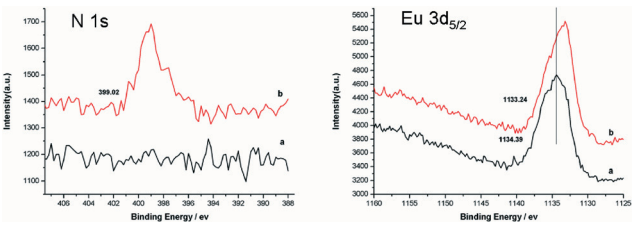

Fig. 5 XPS spectra of N and Eu for (a) EuF_3 and (b) $NH_4Eu_3F_{10}$.

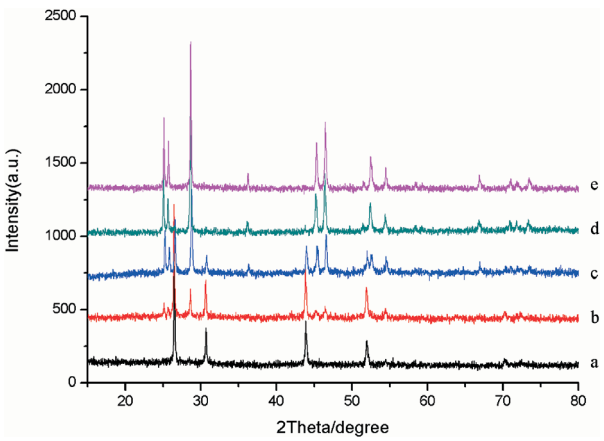

Fig. 6 XRD patterns of products prepared in 5.5 mL of ammonium hydroxide solution for (a) 1 h, (b) 2 h, (c) 3 h, (d) 5 h, and (e) 8 h.

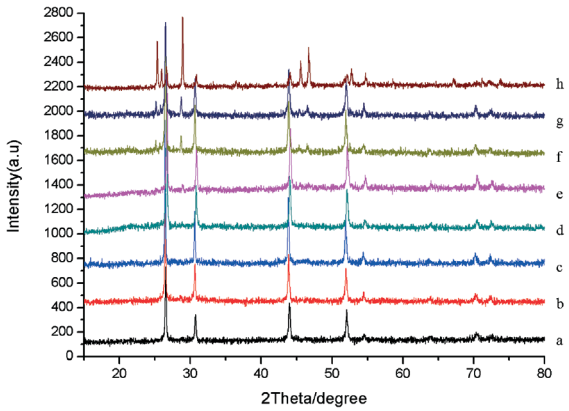

Fig. 7 XRD patterns of products prepared in 9.1 mL of ammonium hydroxide solution for (a) 2 h, (b) 4 h, (c) 6 h, (d) 9 h, (e) 12 h, (f) 13 h, (g) 14 h, and (h) 20 h.

may stabilize $NH_4Eu_3F_{10}$ by affecting the deprotonation of EDTA and oleic acid.

In order to evaluate the influence of EDTA and oleic acid on the final structures, samples were prepared by removing EDTA or oleic acid from the reaction system. $NH_4Eu_3F_{10}$ or a mixture of cubic phase $NH_4Eu_3F_{10}$ and orthorhombic phase EuF_3 was obtained with 5.5 mL of ammonium hydroxide solution after 1 h of hydrothermal treatment without oleic acid or EDTA, respectively (Fig. S1†). Hence, we speculated that EDTA mainly accounted for the stability of $NH_4Eu_3F_{10}$. EDTA chelated Eu^{3+} in our system, which not only controlled the growth of $NH_4Eu_3F_{10}$ nanospheres by decreasing the effective concentration of Eu^{3+}, but also chelating on the surface of $NH_4Eu_3F_{10}$ nanoparticles, thus stabilizing the nanoparticles by reducing the surface energy.

After 1 h of hydrothermal treatment with 5.5 mL of ammonium hydroxide solution, $NH_4Eu_3F_{10}$ nanospheres sized over 200 nm were produced (Fig. 8a), which failed to remain intact after 2 h of reaction (Fig. 8b). Significantly more incomplete nanospheres were discerned when the reaction time was 3 h, with most of them being hollow (Fig. 8c).

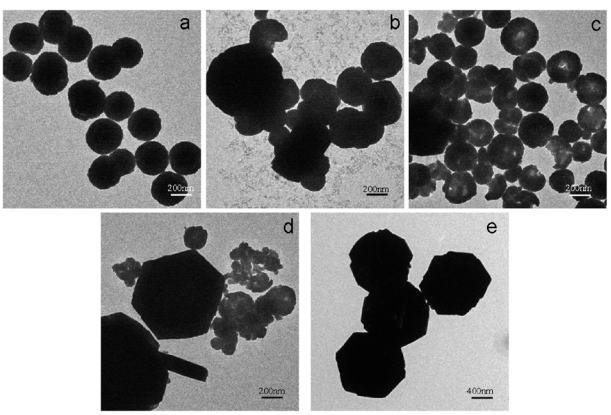

Fig. 8 TEM images of products prepared at 5.5 mL of ammonium hydroxide solution for (a) 1 h, (b) 2 h, (c) 3 h, (d) 5 h, and (e) 8 h.

According to our previous study,[19] these hollow nanospheres, which were hexagonal phase EuF_3, were transformed to hexagonal prisms with extended hydroxide treatment.

However, as the amount of ammonium hydroxide solution was 9.1 mL in this study, $NH_4Eu_3F_{10}$ nanospheres were synthesized in the first 12 h (Fig. 9a–e). EuF_3 hexagonal prisms emerged when the reaction was prolonged to 13 h (Fig. 9f), and no hollow EuF_3 nanospheres formed before 24 h of reaction (Fig. 9h). With 5.5 mL of ammonium hydroxide solution, $NH_4Eu_3F_{10}$ nuclei formed in the beginning, and primary $NH_4Eu_3F_{10}$ particles aggregated to form nanospheres during hydrothermal treatment. With prolonged reaction, $NH_4Eu_3F_{10}$ decomposed as self-sacrificed templates[27] under hydrothermal conditions, and EuF_3 hollow nanospheres formed and transformed into EuF_3 hexagonal prisms according to the oriented attachment mechanism.[28,29] When the amount of ammonium hydroxide solution was raised to 9.1 mL, EDTA was subject to deprotonation, which strengthened the chelation between EDTA and Eu^{3+}, and decreased the effective concentration of Eu^{3+} in the system. As a result, the reaction was decelerated and the as-prepared $NH_4Eu_3F_{10}$ nanospheres were slowly enlarged in the first 6 h (Fig. 9a–c). Due to the effect of strong EDTA chelation, the surface of $NH_4Eu_3F_{10}$ nanospheres dissolved during the long-time hydrothermal treatment, so the size of as-prepared $NH_4Eu_3F_{10}$ nanospheres decreased when the treatment was prolonged to 12 h (Fig. 9e). Hitherto, no EuF_3 hollow nanospheres and hexagonal prisms were discerned. Ligands capped on the surface of nanoparticles were also influenced by pH.[30] As the pH value increased, the chelation between EDTA and Eu^{3+} was strengthened by an increasing dosage of ammonium hydroxide solution. Therefore, more EDTA chelated with Eu^{3+} on the surface of $NH_4Eu_3F_{10}$ nanospheres, which decreased the surface energy of these nanoparticles, thereby further enhancing their thermodynamic stability. Besides, the effective concentration of Eu^{3+} from dissolution of $NH_4Eu_3F_{10}$ did not suffice for EuF_3 nucleation, thus ruling out hollow nanospheres or hexagonal prisms of EuF_3. Dissolution of $NH_4Eu_3F_{10}$ nanospheres with extended reaction eventually allowed EuF_3 formation (Fig. 9f) based on a dissolution–recrystallization process,[31,32] and hollow EuF_3 nanospheres appeared because $NH_4Eu_3F_{10}$ decomposed owing to the thermodynamic instability of the small particles (Fig. 9h).

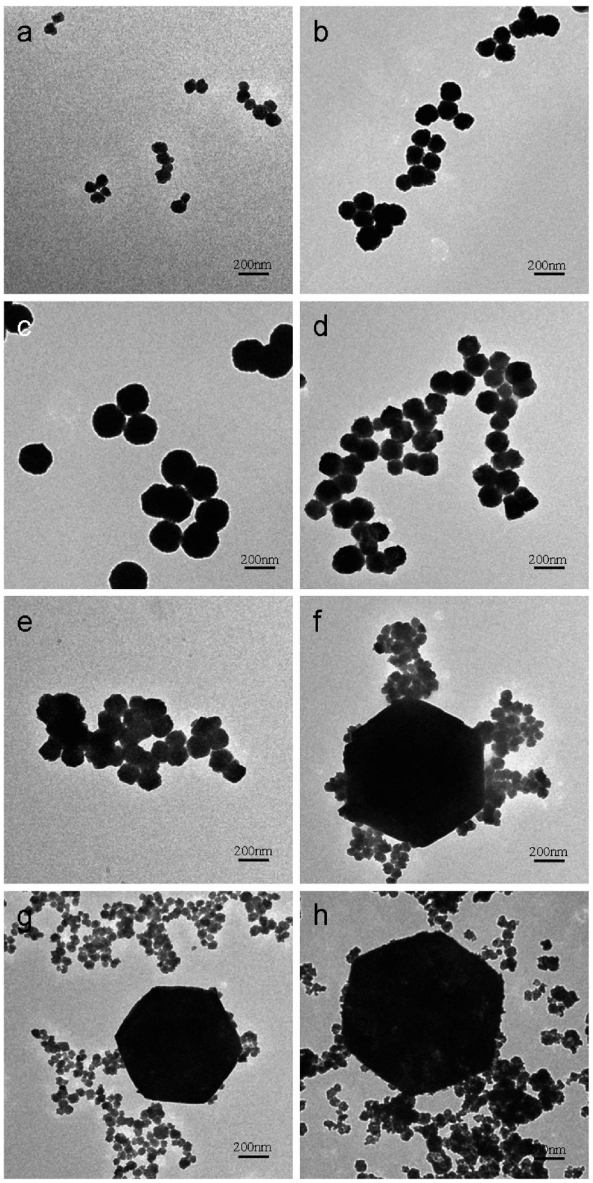

Fig. 9 TEM images of products prepared in 9.1 mL of ammonium hydroxide solution for (a) 2 h, (b) 4 h, (c) 6 h, (d) 9 h, (e) 12 h, (f) 13 h, (g) 14 h, and (h) 20 h.

When the amount of ammonium hydroxide solution exceeded 9.1 mL, a mixture of cubic phase $NH_4Eu_3F_{10}$ and hexagonal phase EuF_3 was obtained after being hydrothermally treated for 8 h (Fig. S2†). Strengthened EDTA chelation promoted the dissolution of $NH_4Eu_3F_{10}$, thus augmenting the effective concentration of Eu^{3+} to the minimum one for EuF_3 nucleation within a short time period. Therefore, excess ammonium hydroxide solution also destabilized $NH_4Eu_3F_{10}$. In short, $NH_4Eu_3F_{10}$ formed in the beginning and then decomposed during the hydrothermal route. Nevertheless, elevating the dosage of ammonium hydroxide solution not only reduced the effective concentration of Eu^{3+}, but also stabilized $NH_4Eu_3F_{10}$ nanospheres by decreasing the surface energy. The $NH_4Eu_3F_{10}$ nanospheres would be much more stable during hydrothermal treatment when the amount of ammonium hydroxide solution was increased reasonably.

The size of $NH_4Eu_3F_{10}$ nanospheres was supposed to be adjusted by changing the amount of ammonium hydroxide solution during short-time hydrothermal treatment. After 1 h of reaction, all the samples were cubic phase $NH_4Eu_3F_{10}$ (Fig. 10). The products were monodisperse with an average diameter of 300 ± 27 nm when 6 mL of ammonium hydroxide solution was used (Fig. 11a), and the average diameter decreased to 177 ± 23 nm with increasing ammonia dosage to 7 mL (Fig. 11b). Nanospheres of diameters about 113 ± 23 nm (Fig. 11c) were obtained when the amount of ammonia was 8 mL. As the dosage was further augmented to 9 mL, the

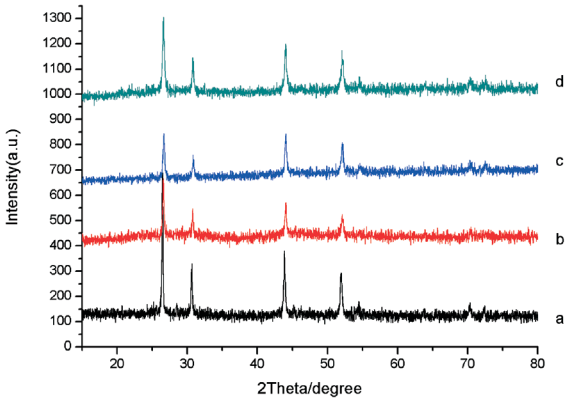

Fig. 10 XRD patterns of products prepared at 110 °C for 1 h with different amounts of ammonium hydroxide solution (a) 6.0 mL, (b) 7.0 mL, (c) 8.0 mL, and (d) 9.0 mL.

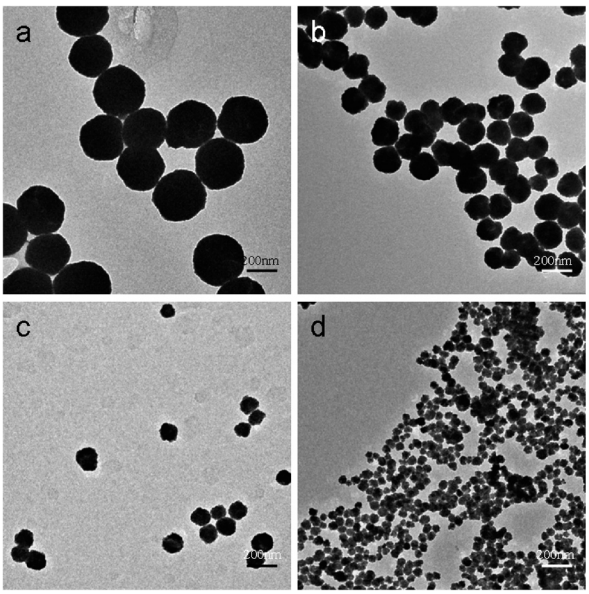

Fig. 11 TEM images of products prepared at 110 °C for 1 h with different amounts of ammonium hydroxide solution (a) 6.0 mL, (b) 7.0 mL, (c) 8.0 mL, and (d) 9.0 mL.

diameter of the nanospheres reduced to 44 ± 11 nm after being hydrothermally treated for 1 h (Fig. 11d).

Down-conversion luminescence spectra of $NH_4Eu_3F_{10}$ nanospheres (Fig. S3†) were measured under room temperature. Upon excitation at 394 nm, the samples emitted intense red light. Emission peaks at 592, 615, 652 and 701 correspond to the $^5D_0$–$^7F_1$, $^5D_0$–$^7F_2$, $^5D_0$–$^7F_3$ and $^5D_0$–$^7F_4$ transitions in Eu^{3+} respectively.[33] The luminescence lifetime of Eu^{3+} in $NH_4Eu_3F_{10}$ nanospheres of 100 nm is 2.18 ms (Fig. S4†), which is longer than that of fluoride[34] and vanadate[35,36] reported before. Although the lifetime of $NH_4Eu_3F_{10}$ nanospheres is shorter than that of phosphate,[37] compared with quantum dots and organic species, these rare-earth doped nanoparticles express much longer luminescence lifetime,[38] which is suitable for time-resolved fluorescence detection *in vitro*. The emission quantum yield of Eu^{3+} in $NH_4Eu_3F_{10}$ nanospheres is 16.2%, which is calculated according to the method reported previously.[34,39–42]

IR spectra were used to identify the capping molecules on the surface of as-prepared $NH_4Eu_3F_{10}$ (Fig. 12). Strong bands at 1630 and 1427 cm^{-1} can be attributed to the asymmetric and symmetric stretching vibrations of bound carboxyl groups,[43] suggesting the binding of EDTA on the surface of nanospheres. The peaks at 2986 and 2856 cm^{-1} correspond to the asymmetric and symmetric stretching vibrations of the C–H bond respectively. The peak at 1712 cm^{-1}, which can be assigned to the C═O asymmetric vibration of the free carboxyl groups of EDTA, represents improved hydrophilicity of as-prepared samples. The peak at 3089 cm^{-1} can be attributed to the C═C–H stretching vibrations of adsorbed oleic acid.

By using MTT assays, we found that the as-prepared $NH_4Eu_3F_{10}$ nanospheres exhibited low cytotoxicity against HeLa cells (Fig. S5†).

Being highly biocompatible and hydrophilic, the as-prepared $NH_4Eu_3F_{10}$ nanospheres are practically applicable after being conjugated with various biomolecules by free carboxyl groups. Nanoparticles of diameter from 10 to 100 nm can easily enter cells, and the as-prepared $NH_4Eu_3F_{10}$ samples are of suitable size and strong luminescence. To test the potential of the as-prepared $NH_4Eu_3F_{10}$ nanospheres in bio-imaging, HeLa cells were incubated with the nanoparticles (prepared in 9.1 mL ammonia for 8 h of hydrothermal treatment) at the concentration of 100 μg mL^{-1} for 0.5–48 h. The images were acquired at the excitation wavelength of 405 nm. After being incubated under experimental conditions for 0.5 h, the cytoplasm of HeLa cells (×10) exhibited intense red emission (Fig. 13a), indicating that the as-prepared nanoparticles entered cells readily. Prolonging incubation enhanced emission in the cytoplasm (Fig. 13b), while extending incubation over 12 h allowed red emission only in the cytoplasm according to the merged fluorescence and bright field images shown in Fig. S6.† The absence of emission in the cell nucleus reveals that the as-prepared large nanoparticles failed to penetrate karyotheca or nucleopores. All results suggest that the as-prepared $NH_4Eu_3F_{10}$ nanospheres are feasible luminescence imaging agents *in vitro*.

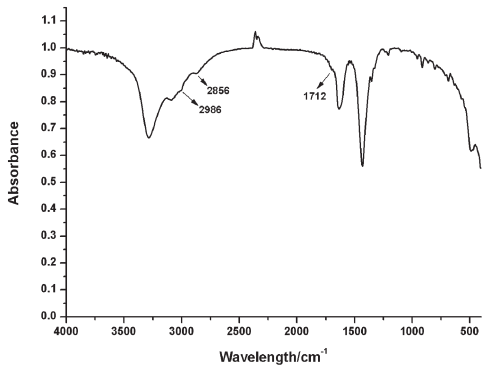

Fig. 12 IR spectra of $NH_4Eu_3F_{10}$ nanospheres.

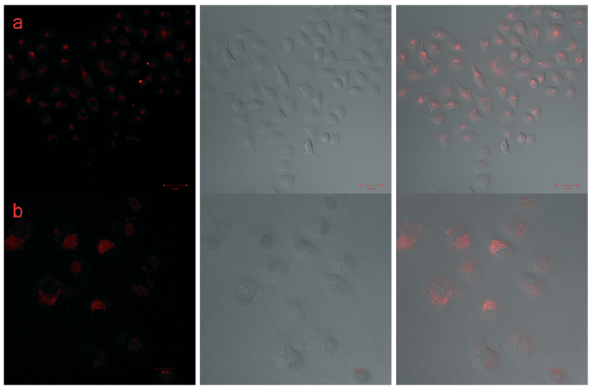

Fig. 13 Excited at 405 nm, CLFM images of HeLa cells stained with 100 μg mL^{-1} $NH_4Eu_3F_{10}$ nanospheres at 37 °C for (a) 0.5 h and (b) 12 h on the left, bright field images in the middle, and merged bright field and CLFM images on the right.

Conclusions

In summary, we herein, for the first time, prepared cubic phase $NH_4Eu_3F_{10}$ nanospheres using a facile modified hydrothermal route. Dependence of the stability of $NH_4Eu_3F_{10}$ nanospheres on the amount of ammonium hydroxide solution and reaction time was investigated. The size of the nanospheres was adjusted by varying the dosage of ammonium hydroxide solution. Furthermore, the nanospheres were used for fast luminescence imaging *in vitro*. The results enrich the field of ammonium rare-earth fluorides and render them potentially eligible for bioimaging.

Acknowledgements

This work is supported by the National Basic Research Program of China (2013CB922102) and the National Natural Science Foundation of China (21075064, 21027013, 21021062, 21275072 and 21201101).

Notes and references

1 M. A. Terekhin, A. N. Vasilev, M. Kamada, E. Nakamura and S. Kubota, *Phys. Rev. B: Condens. Matter*, 1995, **52**, 3117.
2 R. X. Yan and Y. D. Li, *Adv. Funct. Mater.*, 2005, **15**, 763.
3 Z. G. Chen, H. L. Chen, H. Hu, M. X. Yu, F. Y. Li, Q. Zhang, Z. G. Zhou, T. Yi and C. H. Huang, *J. Am. Chem. Soc.*, 2008, **130**, 3023.
4 M. Hyk, R. Kumar, T. Y. Ohulchanskyy, E. J. Beregey and P. N. Prasad, *Nano Lett.*, 2008, **8**, 3834.
5 R. Kumar, M. Hyk, T. Y. Ohulchanskyy, C. A. Flask and P. N. Prasad, *Adv. Funct. Mater.*, 2009, **19**, 853.
6 M. Wang, C. C. Mi, W. X. Wang, C. H. Liu, Y. F. Wu, Z. R. Xu, C. B. Mao and S. K. Xu, *ACS Nano*, 2009, **3**, 1580.
7 L. X. Xie, Y. Qin and H. Y. Chen, *Anal. Chem.*, 2012, **84**, 1969.
8 C. Wang, L. Cheng and Z. Liu, *Biomaterials*, 2011, **32**, 1110.
9 Y. L. Dai, P. A. Ma, Z. Y. Cheng, X. J. Kang, X. Zhang, Z. Y. Hou, C. X. Li, D. M. Yang, X. F. Zhai and J. Lin, *ACS Nano*, 2012, **6**, 3327.
10 F. T. You, S. H. Huang, S. M. Liu and Y. Tao, *J. Solid State Chem.*, 2004, **177**, 2777.
11 S. L. Chamberlain and L. R. Corruccini, *J. Magn. Magn. Mater.*, 2003, **264**, 158.
12 A. Yoshikawa, K. Kamada, M. Nikl, K. Aoki, H. Sato, J. Pejchal and T. Fukuda, *J. Cryst. Growth*, 2005, **285**, 445.
13 S. Aleonard, M. T. Roux and B. Lambert, *J. Solid State Chem.*, 1982, **42**, 80.
14 R. E. Thoma, *Inorg. Chem.*, 1962, **1**, 220.
15 A. Vedrine, R. Boutonnet, R. Sabatier and J. C. Cousseins, *Bull. Soc. Chim. Fr.*, 1975, **3–4**, 445.
16 F. T. You, S. H. Huang, S. M. Liu and Y. Tao, *J. Solid State Chem.*, 2004, **177**, 2777.
17 Z. J. Kang, Y. X. Wang, F. T. You and J. H. Lin, *J. Solid State Chem.*, 2001, **158**, 358.
18 X. Liang, X. Wang, L. Y. Wang, R. X. Yan, Q. Peng and Y. D. Li, *Eur. J. Inorg. Chem.*, 2006, 2186.
19 Z. M. Chen, Z. R. Geng, M. L. Shi, Z. H. Liu and Z. L. Wang, *CrystEngComm*, 2009, **11**, 1591.
20 C. Qin, X. L. Wang, E. B. Wang and Z. M. Su, *Inorg. Chem.*, 2005, **44**, 7122.
21 J. Xia, B. Zhao, H. S. Wang, W. Shi, Y. Ma, H. B. Song, P. Cheng, D. Z. Liao and S. P. Yan, *Inorg. Chem.*, 2007, **46**, 3450.
22 S. P. Sinha, *Struct. Bonding*, 1976, **25**, 69.
23 V.F. Zinchenko, N. P. Efryushina, O. G. Eryomin, V. Y. Markiv, N. M. Belyavina, O. V. Mozkova and M. I. Zakharenko, *J. Alloys Compd.*, 2002, **347**, L1.
24 A. Zalkin and D. H. Templeton, *Acta Crystallogr., Sect. B: Struct. Sci.*, 1985, **41**, 91.
25 A. Arbus, M. T. Fournier, B. Picaud, G. Boulon and A. Vedrine, *J. Solid State Chem.*, 1980, **31**, 11.
26 Z. M. Chen, Q. Zhao, G. J. Feng, Z. R. Geng and Z. L. Wang, *CrystEngComm*, 2012, **14**, 7764.
27 B. X. Li, Y. Xie and Y. Xue, *J. Phys. Chem. C*, 2007, **111**, 12181.
28 D. Winn and M. F. Doherty, *AIChE J.*, 2000, **46**, 1348.
29 P. Hartman and W. G. Perdok, *Acta Crystallogr.*, 1955, **8**, 521.
30 N. Bogdan, F. Vetrone, G. A. Ozin and J. A. Capobianco, *Nano Lett.*, 2011, **11**, 835.
31 A. W. Xu, Y. P. Fang, L. P. You and H. Q. Liu, *J. Am. Chem. Soc.*, 2003, **125**, 1494.
32 J. Lu, Y. Xie, F. Xu and L. Y. Zhu, *J. Mater. Chem.*, 2002, **12**, 2755.
33 M. F. Acosta, R. P. Salas, R. Aceves, M. S. Lerma and R. R. Bon, *Solid State Commun.*, 2005, **136**, 567.
34 L. Zhu, X. M. Liu, J. Meng and X. Q. Cao, *Cryst. Growth Des.*, 2007, **7**, 2505.
35 E. Beaurepaire, V. Buissette, M. Sauviat, D. Giaume, K. Lahlil, A. Mercuri, D. Casanova, A. Huignard, J. Martin, T. Gacoin, J. Boilot and A. Alexandrou, *Nano Lett.*, 2004, **4**, 2079.

36 C. R. Kesavulu, D. G. Lee, S. S. Yi, K. Jang, J. H. Park, J. S. Leem, Y. H. Choi, Y. J. Jang and J. G. Choi, *J. Alloys Compd.*, 2013, **561**, 59.
37 O. Lehmann, K. Kömpe and M. Haase, *J. Am. Chem. Soc.*, 2004, **126**, 14935.
38 J. Sen, L. D. Sun and C. H. Yan, *Dalton Trans.*, 2008, 5687.
39 Z. M. Chen, Z. R. Geng, D. L. Shao, Z. P. Zhou and Z. L. Wang, *CrystEngComm*, 2012, **14**, 2251.
40 C. Y. Peng, H. J. Zhang, J. B. Yu, Q. G. Meng, L. S. Fu, H. R. Li, L. N. Sun and X. M. Guo, *J. Phys. Chem. B*, 2005, **109**, 15278.
41 A. Kar and A. Patra, *J. Phys. Chem. C*, 2009, **113**, 4375.
42 A. Kar, A. Datta and A. Patra, *J. Mater. Chem.*, 2010, **20**, 916.
43 R. Ran, Y. M. Gao, Y. Zheng, K. Wang and Z. P. Shao, *J. Alloys Compd.*, 2010, **491**, 271.